The evaluation of the service life of thermal cut components

Niko Jezernik[1, a], Srečko Glodež[2,b] and Janez Kramberger[3,c]

[1, 2, 3] University of Maribor, Faculty for mechanical engineering,
Smetanova 17, SI-2000, Maribor, Slovenia

[a]niko.jezernik@uni-mb.si, [b]srecko.glodez@uni-mb.si, [c]jkramberger@uni-mb.si

Keywords: plasma cutting, laser cutting, high strength steel, surface roughnes, crack initiation

Abstract. The paper investigates the effects of plasma and laser cutting on the fatigue properties of S960QL high strength steel. High cycle fatigue (HCF) tests were performed at room temperature with constant stress amplitude and axial loading with stress ratio R = 0,1 on specimens manufactured from sheet steel using different cutting speeds. Cut edge quality was defined by grooves left by cutting process and the size and properties of heat affected zone (HAZ). Since in HCF the majority of lifetime of components is spent in crack initiation stage, special attention was given to this phase. A numeric model for crack initiation is proposed and compared to experimental data. The model is based on Tanaka-Mura crack nucleation model while taking cut edge quality (surface roughness and size of HAZ) into account.

Introduction

The investigated steel S960QL (WELDOX 960 E) is commonly used in heavy lifting and similar industries due to its high strength and good weldability. As it is usual for high strength steel, this material is also very susceptible to fatigue, as fatigue strength of this steel typically amounts to half of tensile strength. [1]

The quality of surface also has a considerable influence on the fatigue live of elements. Cutting process itself causes a roughness on the cut edge and also changes microstructural properties of material in heat affected zone (HAZ). Surface roughness, which is usually represented by roughness parameters, such as average roughness height Ra, decreases fatigue life as it causes more stress concentrations and hastens crack initiation. [2-3] Heat input of particular cutting process causes hardening and softening in HAZ and creation of marthensitic layer. This also has an effect of fatigue life, that may be detrimental or beneficial. [4]

Experimental Details

Fatigue testing was performed on four series of thermally cut specimens. PA and PB series were manufactured with plasma with cutting speeds 2120 mm/min and 2400 mm/min. LA and LB series were manufactured with laser with cutting speeds 2430 mm/min and 2700 mm/min

Specimen dimensions were 200 mm × 110 mm × 5 mm (Fig. 1), with a circular hole of 40 mm, that creates a stress concentration with factor K_t = 2,28. Fig. 2 shows how the top (X) and bottom surface (O) of specimens are defined with respect to direction of plasma flow and laser beam.

Tests were carried out on a pulzating machine with uniaxial loading and load control. The stress ratio was R=0,1 with constant stress amplitude. The used frequency of loading was approximately 150 Hz. The specimens were tested in the same state as they were produced and no additional treatment was performed on them. Therefore the properties of cut surface of specimens, most notably roughness and hardness, depend solely upon the parameters of the cutting process. Each series of 6-9 samples was loaded at different stress levels ranging from 435 to 660 MPa (K_t taken into account). Stress loads were chosen so as to evaluate high cycle fatigue range from 10^5 to 2×10^6 cycles.

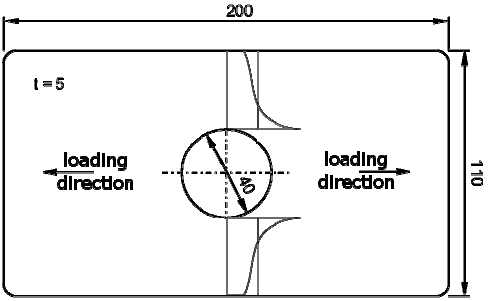

Figure 1: Specimen dimensions

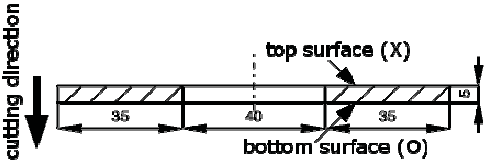

Figure 2: Cross-section of specimen through circular hole showing top and bottom surface with respect to direction of plasma flow or laser beam

Surface Roughness

Surface roughness was determined using a perthometer. Since the expected roughness is in range 5<Ra<10, reference measurement length was chosen to be 12,5 mm. Fig. 3 shows cut edges of two specimens cut with plasma and laser, while figure 4 shows profiles of cut edges these edges as detected by profilometer. Contrary to our expectations specimens cut with laser visually appear to have rougher edge than plasma cut specimens, probably because the cut edge grooves of laser cut specimens are more closer spaced than edge groves of plasma cut specimens (Fig. 3 and 4).

As is expected, a higher cutting speed causes a rougher cut surface.

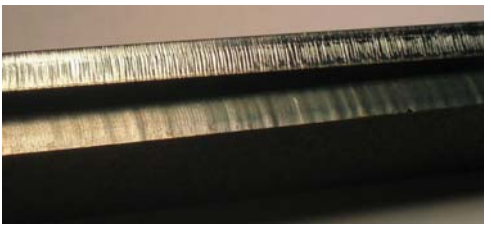

Figure 4: A comparison of cut edges cut with laser (top) and plasma (bottom)

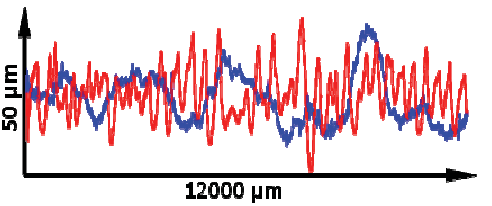

Figure 3: Cut edge profiles of plasma (blue) and laser (red) as detected by perthometer

Results of roughness analysis are shown in table 1. Higher cutting speed caused a small increase in roughness in plasma cut specimens, but is far more influential in case of laser cutting.

Table 1: Comparison of roughness parameters

	PA (2120 mm/min)	PB (2400 mm/min)	LA (2430 mm/min)	LB (2700 mm/min)
Ra	5,1	5,8	5,0	9,1
R_{max}	28,3	35,2	37,6	49,3

Micro-hardness

Heat input due to cutting process causes metallographic changes in the HAZ of elements. The depth of this layer was evaluated by measurements of micro-hardness with a 0,5 kg load.

Measurements were taken starting 50 µm from the cut edge and ending 1 mm deep. Both top and bottom surface were inspected this way. For plasma cut specimens measurements were taken in 50 µm intervals, but for laser cut specimens measurements were done in 25 µm intervals, because of much narrower heat affected zone. In order to get more consistent results with less variance, three separate measurements were taken and averaged at each depth.

Table 2 shows a comparison of minimum and maximum micro-hardness along top (X) and bottom (O) surfaces of specimens.

Table 2: Comparison of micro-hardness

	PA (2120 mm/min)		PB (2400 mm/min)		LA (2430 mm/min)		LB (2700 mm/min)	
	HV	depth [μm]	HV	depth [μm]	HV	depth [μm]	HV	depth [μm]
max X	482	300	486	250	491	175	496	150
min X	321	450	327	400	318	275	315	250
max O	471	250	489	200	492	125	493	100
min O	312	450	318	350	319	225	324	200

Fig. 8 shows the course of micro-hardness from the cut edge toward interior, across the top surfaces of different series specimens. It is evident that the HAZ of laser cut specimens (LA and LB) is much smaller then HAZ of plasma cut specimens (PA and PB). This is most notable when LA an PB series are compared. Both series are cut with nearly the same speed yet HAZ of laser cut series is significantly narrower. Similarly, a higher cutting speed, while using the same cutting process, also results in narrower HAZ.

The difference in micro-hardness of top and bottom surfaces for plasma cut specimens are presented in fig. 9. The bottom surfaces (PAO and PBO) have somewhat HAZ then the top surfaces (PAX and PBX). The same is also true for laser cut specimens.

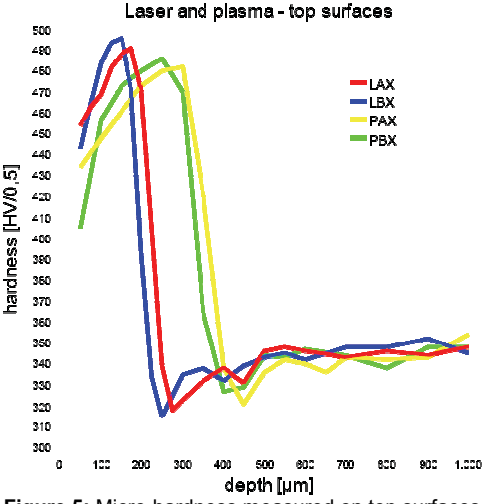

Figure 5: Micro-hardness measured on top surfaces of laser and plasma cut series

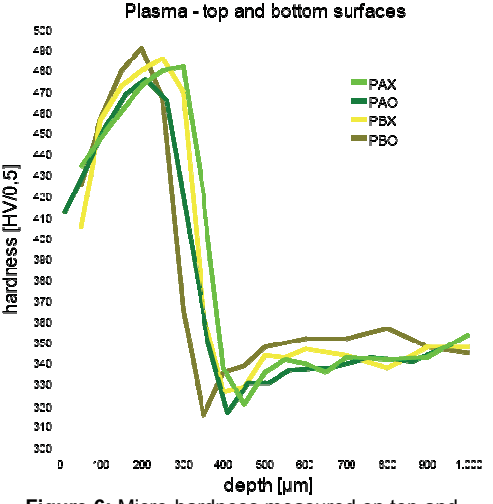

Figure 6: Micro-hardness measured on top and bottom surface of plasma cut specimens

Experimental Results

In all cases cracks formed, as expected, at the inner hole (Fig. 1), where highest stresses are present due to stress concentration factor K_t. In plasma cut specimens a crack typically formed at the bottom surface of specimen (Fig. 7) and also propagated faster along the bottom surface. This indicates an elliptic crack front that originated in one point. This feature was not observable in case of laser cut specimens where cracks propagated equally fast along both sides, indicating a strait crack front parallel to cut surface(Fig. 8).

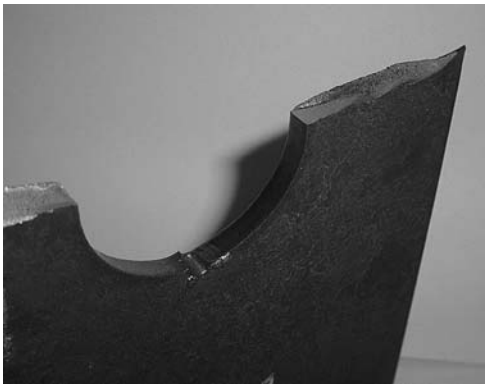

Figure 7: Plasma cut specimen

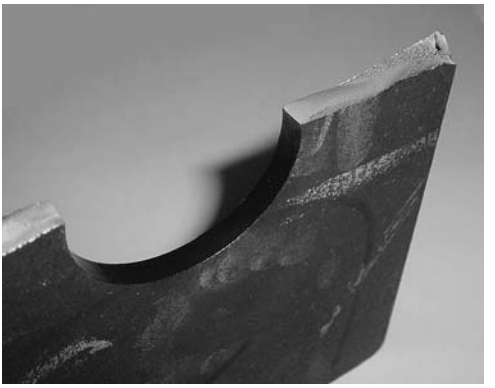

Figure 8: Laser cut specimen

Fig. 3 shows the experimental fatigue life data for all series of specimens in a log-log graph. Best fit Wöhler curves are also included in diagram. Since only one test was carried out for each load level, we were not able to statistically evaluate the data and assess its reliability. Nevertheless exponents of fatigue strength-b have been calculated while assuming that coefficient of fatigue strength ($\sigma_f^{'} = 1167\text{MPa}$) is equal for every specimen (see table 3).

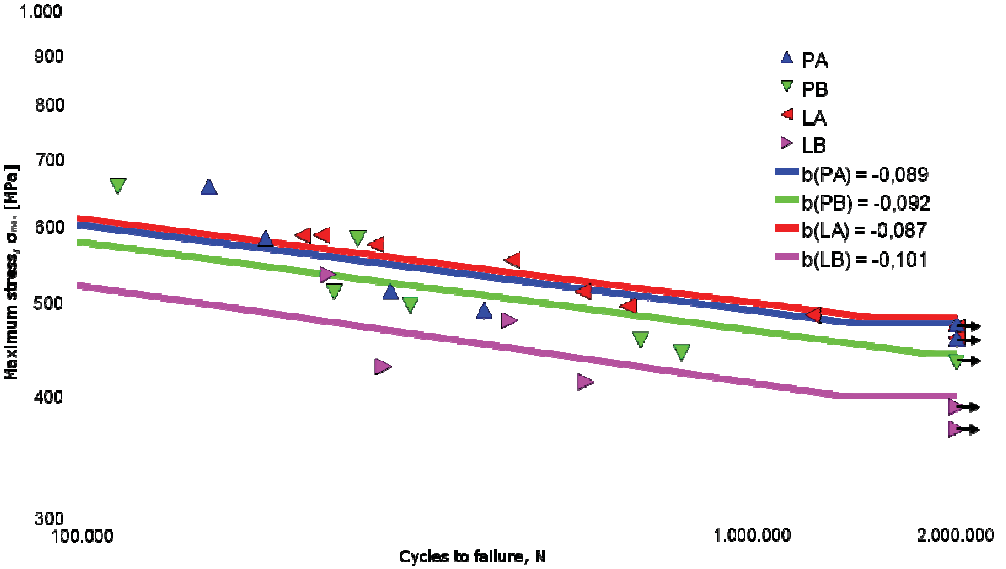

Figure 9: Experimental results with appropriate Wöhler curves

Table 3: Results

	PA (2120 mm/min)	PB (2400 mm/min)	LA (2430 mm/min)	LB (2700 mm/min)
Ra	5,1	5,8	5,0	9,1
b	-0,089	-0,092	-0,087	-0,101
fatigue limit [MPa]	475	440	485	400

Crack Nucleation

As it is common in high cycle fatigue, crack initiation represents a majority of total service life. Furthermore, crack initiation, as well as early short crack growth, highly depend on the microstructure of material, therefore a local approach is needed. Fig. 10 shows a sub model (0,5x0,5 mm) that was used in this manner. Sub model was created in place where there are highest stresses (at the inner hole – Fig. 11) and formation of cracks is expected. Boundary conditions (red borders) were applied as calculated in full scale model. In this sub model a randomly generated Voronoi tessellation was created so as to simulate individual grains. This grains were given randomly oriented orthotropic material properties of marthensite (C11 = C22 = C33 = 233 Gpa, C12 = C13 = C23 = 135 GPa, C44 = C55 = C66 = 118 GPa). [5] For crack nucleation a Tanaka-Mura model (Eq. 1) was used. [6]

$$N_c = \frac{8GW_s}{\pi(1-v)d(\Delta\tau - 2k)^2} \tag{1}$$

This model presumes that cracks form along the slip bands of grains depending on slip band length d, and average shear stress range on the slip band $\Delta\tau$. Other material parameters are: shear modulus G = 118 GPa, specific fracture energy per unit area Ws = 2,0 kJ/m^2, Poisson's ratio υ = 0,3, and frictional stress of dislocation on the slip plane k = 108 MPa.

Fig. 11 shows shear stresses in said sub model where a few micro cracks have already been formed (white lesions). It is evident that shear stresses deviate significantly between grains, depending on particular grain orientation and existence of nearby micro-cracks. When a sufficient amount of micro-cracks occur they coalesce in a macro crack, that can be used as an initial crack for a standard fracture mechanic model.

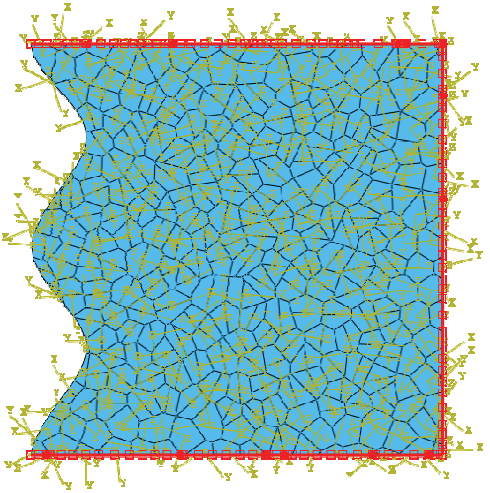

Figure 11: Sub model with randomly oriented grains

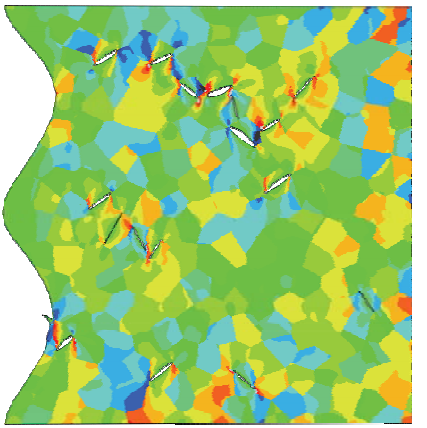

Figure 10: Shear stresses in sub model

Damage Accumulation

Crack nucleation can be evaluated in multiple iterations. Firstly shear stress distribution in sub model is calculated. Then for each grain the number of cycles till micro-crack formation is calculated using Eq. 1. In the grain with the smallest number of cycles a micro-crack is introduced,

which causes stress relaxation in that grain and different stress distribution in surrounding grains. The changed model serves as input for the next iteration.

The problem with this approach is, that in each iteration the number of cycles for each grain is calculated anew, without any consideration of previous states. In this respect a slightly modified approach is proposed, that considers damage accumulation in every iteration.

Firstly total damage, needed for crack nucleation in every grain is calculated using Eq. 2.

$$TD = 8\pi(1-\nu)dGW_s \tag{2}$$

Then for each iteration (marked by index *i*) partial damage in each grain is calculated (Eq. 3).

$$PD_i = (\Delta\tau_i - 2\mathrm{k})^2 \tag{3}$$

The number of cycles, required for micro-crack formation, is calculated (Eq. 4). *TD* and *AD* represent total damage and accumulated damage of particular grain.

$$N_i = \frac{TD - AD}{PD_i} \tag{4}$$

In next iteration a micro crack is introduced in the grain with the smallest N_i and the accumulated damage of other grains is increased for $PD_i \cdot N_{i,min}$.

Numeric Example

Fig. 12 shows a comparison between empiric and numeric results for LA series. This series was chosen for example, because the empiric data of this series shows the least amount of scatter among all series. Also, laser cut series feature a strait crack front that can be more accurately modeled with a 2D model than elliptic crack of plasma cut series.

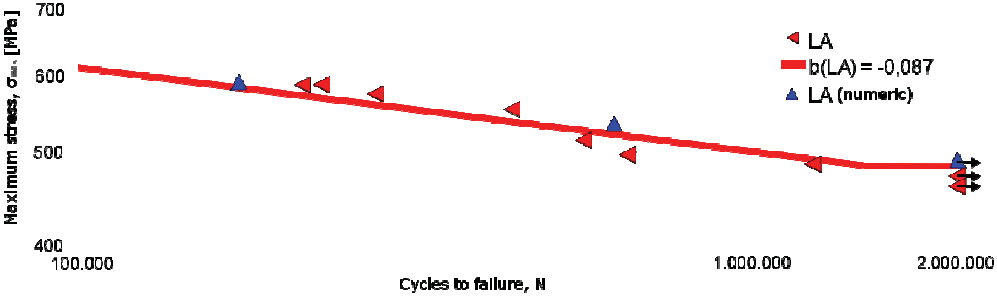

Figure 12: Comparison of empiric and numeric results

Numeric simulation was done on three load levels: 590, 510, and 490 MPa. Sub model was created with a roughness profile of the same amplitude and period as it was obtained by perthometer (Fig. 4). The width of sub model was the same as the width of marthensitic layer in HAZ (Fig. 5).

Sub model was ran through so many iterations that numerous micro-cracks formed a line through the width of sub model and crack nucleation was considered to be finished (Fig. 11). The size of this line was used as an initial crack for regular fracture mechanics model. The numeric results presented in fig. 12, consist of combined crack initiation and crack propagation part (see table 4).

In case of lowest load (490 MPa) only a few scattered micro-cracks were formed during crack initiation phase, implying that no formation of macro-crack will occur and that fatigue limit has been reached.

Table 4: Initiation and propagation cycles for different load levels

load level [MPA]	590	510	490
initiation cycles	136.000	561.000	∞
propagation cycles	34.000	47.000	/
total cycles	170.000	608.000	∞

Conclusion

In the paper, the effects of different cutting speeds on fatigue life of high strength steel were presented. Variations of cutting speed result in different edge quality, that affect crack initiation stage. In this manner surface roughness and the size of heat affected zone are investigated. Experimental high cycle fatigue tests have shown a strong correlation between surface roughness and reduced fatigue life.

A numeric model, based on Tanaka-Mura crack nucleation model, is presented. The model simulates the effects of micro-structure and micro-crack formation along slip bands of grains. Damage accumulation of irreversible slip on slip bands is is also considered.

The numeric model exhibits strong correlation with experimental data but still has some deficiencies. Model doesn't provide a good criteria for micro-cracks coalescence into a macro-crack. In this manner the model should be adapted, perhaps to allow extension of micro-cracks through grain boundaries.

References

[1] G. Pusch, P. Hübner, Bruchverhalten des StahlesStE StE 960 und seiner Schweisswerbindung bei statischer und zyklischer Belastung, Luxemburg: Amt für Veröffentlichungen der Europäischen Gemeinschaften.

[2] Z. F. Yue, Surface roughness evolution under constant amplitude fatigue loading using crystal plasticity, Engineering Fracture Mechanics 72 (2005) 749-757.

[3] F. V. Antunes, A, Ramalho, J. M. Ferreira, Identification of fatigue crack propagation modes by means of roughness measurements, International Journal of Fatigue 22 (2000) 781-788.

[4] C.A. Rodopoulos, E.R. de los Rios, Theoretical analysis on the behaviour of short fatigue cracks, International Journal of Fatigue 24 (2002) 719–724.

[5] Xinyue Huang, Angelika Brückner-Foit, Michael Besel, Yasuko Motoyashiki, Simplified three-dimensional model for fatigue crack initiation, Engineering Fracture Mechanics 74 (2007) 2981–2991.

[6] S. Meyer , A. Brückner-Foit, A. Möslang, Yasuko Motoyashiki, A stochastic simulation model for microcrack initiation in a martensitic steel, Computational Materials Science 26 (2003) 102–110.